Energetics and Kinetics of the Physisorption of Hydrocarbons on Au(111)

S. M. Wetterer, D. J. Lavrich, T. Cummings, S. L. Bernasek,* and G. Scoles*

Department of Chemistry and Princeton Materials Institute, Princeton University, Princeton, New Jersey 08544

Received: May 22, 1998; In Final Form: September 9, 1998

Helium atom reflectivity has been used to study the adsorption of a series of *n*-alkanes, 1-alkenes, and cyclic hydrocarbons on a Au(111) surface. Using this technique, both adsorption and desorption could be observed with high sensitivity under UHV conditions to determine adsorption energies and initial sticking coefficients. For the long-chain *n*-alkanes studied ($C_6H_{14}-C_{12}H_{26}$), the physisorption energy increases linearly with the chain length by 6.2 ± 0.2 kJ/mol per additional methylene unit. The physisorption energies of the 1-alkenes ($C_6H_{12}-C_{11}H_{22}$) show a similar linear dependence on chain length but are slightly higher than those of the corresponding alkanes. A bond-additive model is presented which is capable of predicting the adsorption energy of 25 saturated and unsaturated hydrocarbons on the basis of four fitted parameters with an average error of 1.9%. Of the molecules considered, 84% of the calculated adsorption energies differ from the experimental value by less than twice the average error. When 10 sulfur-containing compounds and two fitting parameters are added, the average error grows to 2.6%. For all linear hydrocarbons studied, the physisorption sticking coefficient is a function of the reduced surface temperature T^*, which is defined as the temperature measured in units of the peak desorption temperature as observed by temperature programmed desorption. The sticking coefficient of each species is close to unity at low temperatures, starts to decrease at $T^* = 0.8$, and reaches zero as the crystal temperature approaches the peak desorption temperature.

1. Introduction

The study of the adsorption of hydrocarbons on transition metal surfaces has been a focal point of surface science research for several decades. Using single crystals and precisely controlled deposition conditions, a variety of molecule−surface interactions have been studied.[1] Depending on surface temperature and other experimental parameters which determine the available free energy, hydrocarbons can chemisorb, physisorb, or react with adsorbates already on the surface.

Hindered by the presence of activation barriers and by steric requirements, direct dissociative chemisorption generally cannot readily occur at low surface temperatures. While hydrocarbons are not observed to chemisorb on Au(111) under moderate conditions,[2] investigations of the rate of dissociative adsorption for short alkanes on other more active, low-index metal surfaces (e.g., Ir(110)[3], Pt(111),[4] Ni(110), and Ni(111)[5]) have shown the activation energy for chemisorption to range from 10 to 50 kJ/mol. To provide enough energy to overcome the barrier to direct chemisorption, either the surface temperature or the translational energy of the incident molecule can be increased. Alternatively, chemisorption can be achieved through a physisorbed precursor-mediated process.

By lowering the surface temperature, a stable coverage of physisorbed molecules can be generated. While in a bound state, each molecule is held in relative proximity to the surface (typically 3.3−3.9 Å for hydrocarbons[6,7]) for a period much longer than the few picoseconds of a single elastic or mildly inelastic surface encounter. Although less free energy is available to the molecule at lower surface temperatures to overcome the same chemisorption barrier, the adsorbates are able to make many more attempts at chemisorption before desorbing. Since the chemisorption rate is related to the population of adsorbates and the residence time, the rate of precursor-mediated chemisorption will be seen to *decrease* when the surface temperature is increased.[8] For large molecules that are still capable of physisorption at high surface temperatures where available free energy is sufficient to overcome the barrier, this precursor-mediated pathway may be highly effective.

At low surface temperatures ($T_s < 200$ K for small molecules) and low incident molecular translational energies, hydrocarbons have been observed to physisorb molecularly even on reactive metal surfaces. Low-temperature studies of the adsorption of alkanes on Cu(100),[9] Pt(111),[10,11] Pt(110),[12] Ir(110),[13] and Ru(001)[14] have measured physisorption energies at partial and full monolayer coverages. Although exact adsorption energies differ slightly due to the atomic structure and the surface potential of the metal substrate, a linear dependence of the adsorption energy on chain length is generally observed (Figure 1). The measured energies are proportional to such molecular properties as the polarizability and the bulk enthalpy of vaporization of the adsorbate indicating that dispersion forces are primarily responsible for the physisorption well depth.

While it is found that the incremental bulk heat of vaporization per additional methylene group is 5 kJ/mol for the physisorption of linear alkanes on Cu(100)[9] or Ru(001),[14] the incremental desorption energy per methylene is 6.5 kJ/mol. A recent study of the adsorption of several hydrocarbons with less than seven carbon atoms on Cu(100)[15] has found that (a) the incremental adsorption energy per methylene unit is 6.3 kJ/mol, (b) the cyclic hydrocarbons need less energy to evaporate than the corresponding linear alkanes, and (c) the alkenes need on the order of 4 ± 1 kJ/mol more energy to desorb than the corresponding saturated compounds. Only one study reported to date has quantified the adsorption of alkanes on Au(111),

* To whom correspondence should be addressed.

10.1021/jp982338+ CCC: $15.00
Published on Web 10/21/1998

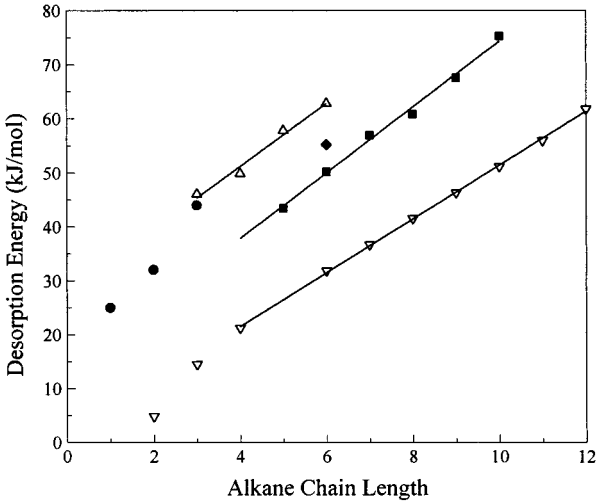

Figure 1. The desorption energies determined by temperature programmed desorption are shown for alkanes deposited on a variety of surfaces: Cu(100)[9] (◆), Pt(111)[10,18] (●), Ru(001)[14] (△), and Au(111)[16] (◆). The enthalpy of vaporization (▽) is also shown for comparison.[39]

yielding for the physisorption energy of *n*-hexane the value of 55.2 kJ/mol[16] which is similar to the data obtained on other surfaces.

As part of a larger study on the self-assembly of 1-alkanethiols on Au(111),[17] the physisorption and chemisorption of a series of sulfur-containing molecules have been separately characterized. In the course of that study, it became necessary to obtain the physisorption energies of several *n*-alkanes on Au(111) as a benchmark reference. To complement the linear alkane data, the study was then expanded to a series of alkenes and to several cyclic molecules with various structures. The results are reported here together with a bond-additive model that not only rationalizes the data but also has predictive value. In addition, the initial sticking coefficients were determined for the adsorption of the longer-chain, linear alkanes on a Au(111) crystal, at surface temperatures between 200 K and the desorption temperature of each hydrocarbon. Sticking coefficients have previously been reported only for small alkanes on Pt(111).[18,19] These kinetic results are also examined in the light of existing quantitative models of surface condensation.[20]

2. Experimental Section

To determine surface coverage, most of the experiments performed in this study have utilized a relatively uncommon technique: helium atom reflectivity. When probed with a collimated helium beam, a close-packed metal surface behaves like a mirror. If the single-crystal surface is clean and well-annealed, the specular reflection signal will be quite strong, indicating a high degree of order. However, if the surface is contaminated with adsorbates or contains defects, the reflection signal will be less intense. Thus, a decay in the intensity of the specular reflection signal is observed when the clean crystal surface is covered with adsorbates. In principle, when enough molecules have adsorbed to complete a monolayer, the return of order may cause the specular signal to recover. However, the likely presence of structural defects in the organic monolayer, the much larger molecular corrugation of the adlayer, as well as the higher probability of inelastic collisions, will make the specularity of the complete hydrocarbon overlayer significantly less than that for the clean metal surface.

Using this technique, sensitivity to adsorbate molecules at low coverage is extremely high. Since the loss of specular intensity results from any event which causes diffusive scattering, attractive interactions with adsorbate molecules at distances more than twice their repulsive diameters are sufficient to deflect the helium atoms away from the specular direction.[21] Typically, this response can be seen experimentally in effective adsorbate cross-sections at low coverage that are many times larger than their expected hard-sphere cross-sections.[22]

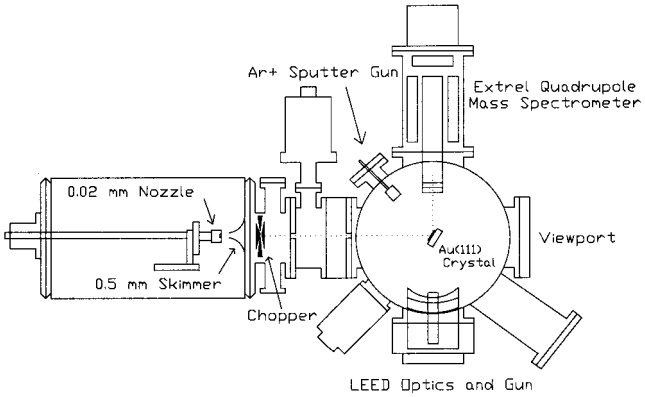

Figure 2. Overview of the experimental apparatus used in these studies. Pumping (not shown) is provided by a VHS-6 diffusion pump (3000 L/s) in source chamber, a TMP-360H turbopump (400 L/s) in the 1st differential chamber, a TPU-170 turbopump in the 2nd differential chamber, and two TMP-340M turbopumps (450 L/s, each) in the scattering chamber.

As the coverage increases, the overlap of the scattering cross-sections of the individual adsorbates will affect the rate of specular decay provided by each additional adsorbing molecule. For molecules that adsorb at random locations, the likelihood of random overlap increases with coverage thus reducing the effective cross-section.[23] If the molecules do not adsorb completely randomly but instead are constrained to adsorb preferentially on substrate lattice sites, the increased spacing of adsorbates will limit the degree of overlap possible and a slower decay of effective cross-section will be observed.[24] In contrast, adsorbate molecules that repel each other will not exhibit any overlap and will show a constant effective cross-section. Alternatively, if the hydrocarbons migrate and form islands upon adsorption, the effective cross-section will also be constant (and smaller) throughout the dosing since each additional molecule will occupy an island edge position. As a result, the degree of interadsorbate attraction or repulsion can be determined experimentally by observing the change in effective cross-section as a function of increasing coverage.

2.1. Apparatus. A molecular beam instrument was assembled to perform both helium atom reflectivity measurements and reflectivity detected temperature-programmed desorption under ultrahigh vacuum conditions. (Figure 2) The machine is composed of two sections separated by a gate valve: (a) a bakeable scattering chamber for preparation of, experimentation with, and long-term clean storage of the Au(111) crystal and (b) a turbopumped beamline where a high-intensity, collimated helium beam is generated by extracting the core of a high-pressure helium expansion through two stages of differential pumping.

The probe beam is generated by the supersonic expansion of 2 MPa of zero grade helium (Airco, 99.997% minimum purity) from a 20 μm diameter nozzle held at room temperature. To maximize the beam flux, the position of the nozzle assembly can be adjusted under vacuum by means of a stepper motorized $x-y-z$ translation stage. A 0.5 mm diameter skimmer located 15 mm away from the nozzle injects the core of the expansion into the first of two differentially pumped chambers. Two

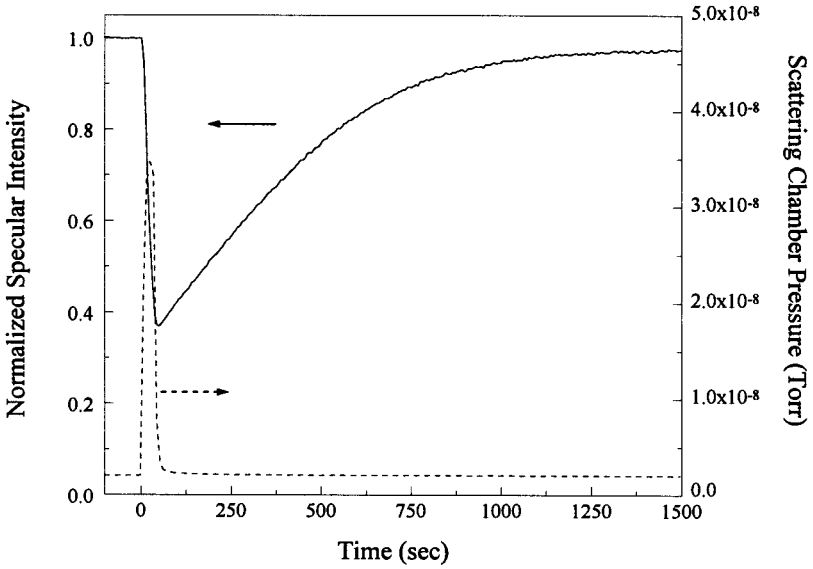

Figure 3. An example of a dose-desorption run showing the decrease and subsequent recovery of the specular intensity (—, left axis) from a Au(111) crystal held at 220 K. The chamber pressure (— —, right axis) resulting from introduction of *n*-heptane to the scattering chamber is shown. Chamber pressure was not corrected for the ion gauge sensitivity to helium ($S/S_{N2} \cong 0.15$) or heptane ($S/S_{N2} \cong 7.0$).

collimator plates with 3 mm diameter apertures located at the end of each differential chamber at respectively 10 and 22.5 cm from the nozzle further reduce the lateral size of the beam. At the crystal, located 45.7 cm from the nozzle, the beam is approximately four mm in diameter and has an intensity of about 10^{14} atoms/cm^2•s.

Pumping along the beam line is provided by an unbaffled 6000 L/s VHS-6 diffusion pump, a 360 L/s TMP-360 turbopump, and a 170 L/s TPU-170 turbopump in the source, first differential, and second differential chambers, respectively. Typical helium loads during experiments generate pressures of up to 1×10^{-4} Torr in the source chamber, 1×10^{-6} Torr in the first differential chamber, and 1×10^{-7} Torr in the second differential chamber. In the crystal manipulation chamber, a pair of 450 L/s TMP-340M magnetic bearing turbopumps maintain UHV ($\leq 1 \times 10^{-10}$ Torr) when all gas sources are off and a pressure of 2×10^{-8} Torr when the helium beam is admitted to the scattering chamber.

Modulation of the beam is provided by a four-vane chopper wheel located 8 cm from the nozzle. Typically, the beam is chopped at 340 Hz with a 50% duty cycle. The chopping frequency is measured by an infrared LED-photodetector assembly and used as a reference signal for a lock-in amplifier. In addition, a solenoid operated flag located in the first differential chamber is also available to interrupt the beam for long periods of time.

Fixed at a right angle to the beamline, the ionizer of an Extrel quadrupole mass spectrometer used for beam detection is located 6 cm from the center of the scattering chamber. The gold crystal (purchased from Aremcoproducts, Inc.) was polished, etched, and annealed until the exposed face was optically smooth and oriented within 0.3° of the (111) plane as determined by X-ray diffraction. For proper alignment with both the beam source and the mass spectrometer detector, the crystal is secured on a six degree-of-freedom adjustable mount ($x, y, z, \theta, \phi, \rho$) located in the center of the scattering chamber. A 40 W cartridge heater mounted behind the sample and a liquid nitrogen reservoir connected to the sample mount by a copper braid provide temperature control up to 1000 K. The sample temperature was monitored using a chromel−alumel thermocouple clamped between the gold crystal and the sample mount.

To ensure cleanliness before each experiment, the sample was heated to 850 K and bombarded with 3 keV argon ions for a period of at least 15 min. Following a 10 minute annealing period with the temperature maintained at 850 K, the helium beam specular intensity was measured. If the resulting specular intensity corresponded to the 30% reflectivity generally observed for clean Au(111) surfaces, the sample was judged to be clean. Typically, additional cleaning of the crystal has not been observed to produce higher specular intensities than those obtained with this 25 min cycle. As a result, typical hydrocarbon dose−desorb−clean experimental cycles can be performed in 1 h or less.

Dose molecule samples were purchased from Aldrich Chemical Corporation. For the *n*-alkanes, sample purity was typically in excess of 99%. For the 1-alkenes, the purity ranged from 94 to 99% with most impurities due to the presence of alkanes of similar chain length. These samples were stored at room temperature in a stainless steel tube for periods not in excess of 2 weeks. Removal of atmospheric gases introduced during the loading procedure was achieved by repeated freeze−pump−thaw cycles until no additional impurity gases evolved from the sample container during the pump cycle.

A few of the molecules studied here, i.e., those with an activation energy for desorption smaller than 50 kJ/mol, required lower surface temperatures which could not be easily achieved in this apparatus. Reflectivity-detected TPD measurements for these molecules were carried out in the helium beam surface diffraction facility available in our laboratory. This diffraction apparatus, which has been described in detail elsewhere,[25,26] works in a very similar way as the one described here and can achieve surface temperatures as low as 40 K but is not suitable for helium atom reflectivity measurements at surface temperatures above room temperature.

2.2. Experimental Procedures. To perform a helium atom reflectivity experiment, the gold crystal is oriented with its surface normal at 45° with respect to the primary beam to direct the specular reflection into the mass spectrometer. After stabilization of the helium beam and the crystal surface temperature, data acquisition begins by establishing a clean gold specular signal intensity (I_o). Dosing is achieved by the release of hydrocarbon vapor through a leak valve at the base of the

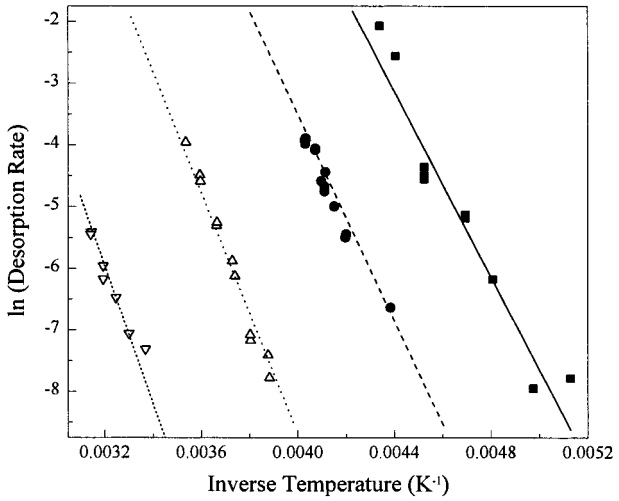

Figure 4. Sample Arrhenius plots of experimentally determined desorption rates for four alkanes: heptane (◆), octane (●), decane (△), and dodecane (▽). Slopes correspond to the energy of desorption while the *y*-intercept provides the preexponential factor (typically $\sim 10^{13}$).

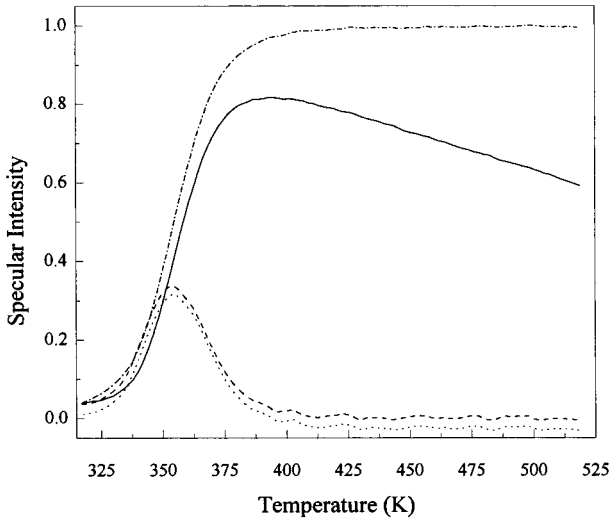

Figure 5. Processing of specular intensity data (—) from a helium specular TPD experiment with dodecane is shown. After a correction for Debye−Waller effects(−·−·), differentiation of resulting curve provides a traditional TPD "peak" (− −). If the Debye−Waller correction is not applied (···), the peak location does not shift significantly.

scattering chamber. A diffuser plate mounted inside the chamber prevents the molecules from traveling along a direct line of sight path to the crystal. As the molecules stick to the surface, they diffusely scatter some of the incident helium beam and the specular signal decreases. If the adsorption and desorption rates are balanced, a steady-state population is formed and the specular signal intensity stabilizes. When the dosing is interrupted, desorption of adsorbates can be observed as a recovery of specular signal. During an experiment, dose fluxes were maintained low enough to prevent detectable attenuation of the helium beam by ambient gas in the scattering chamber.

From simple dose−desorption experiments (Figure 3), both the initial drop and subsequent recovery of specular signal provide useful information. At the onset of dosing, the adsorption rate can be determined by conversion of the measured decay of specular signal to an increase in absolute coverage. With the impingement rate calculated from the measurement of the partial pressure of the hydrocarbon vapor in the scattering chamber, a sticking coefficient can also be generated. After dosing is stopped, the measurement of the half-life of the specular recovery provides the desorption rate. When a set of desorption rates for different temperatures is obtained, an Arrhenius plot of ln(rate) as a function of inverse temperature can be formed (Figure 4). The slope of the best-fit line through these points is related to the energy barrier for desorption with the *y*-intercept equal to the natural logarithm of the preexponential factor.

To confirm the magnitude of the activation energy for desorption as determined by the Arrhenius desorption rate plot, a second set of experiments was carried out using temperature programmed desorption (TPD). Following deposition at surface temperatures which were low enough to maintain an adequate adsorbate coverage, desorption was monitored using either the traditional method of measuring the partial pressure of desorbing species, or the more sensitive helium atom reflectivity. The temperature of the crystal was ramped at a rate of 1−5 K/s during desorption. Since the helium beam is only sensitive to adsorbates on the crystal surface, errors which may arise from contributions to the traditionally detected TPD signal generated by the outgassing of the sample mount are avoided.[27] In addition, the high sensitivity of helium scattering allows for the observation of the desorption of populations too small to be detected using traditional TPD. Although observation of multilayer desorption or identification of desorbing species is not possible using helium atom reflectivity, monitoring thermal desorption in this way is a useful complement to traditional TPD.

To determine the peak desorption temperatures using this approach, the mass spectrometer is tuned to $m/e = 4$ during the temperature ramp. To correct for the loss of specular intensity at higher surface temperatures due to inelastic scattering (Debye−Waller attenuation[28]), the recorded helium reflectivity curve is normalized against a curve of the reflectivity of bare gold measured over the same temperature region. (Although this correction does not significantly affect peak location, it can reveal small, high-temperature desorption events that are obscured by the attenuation.) When the resulting curve is differentiated, a set of "desorption peaks" is generated which correspond to temperatures of greatest desorption rate (Figure 5). Due to the large effective scattering cross-section of the adsorbates, only the desorption of the last ∼20% of the monolayer is observed by reflectivity detected TPD. Although the amplitude of the peaks generated by this procedure may differ from those observed using traditional TPD, the temperature positions are identical within experimental error. For both TPD techniques, desorption temperatures are converted to activation energies for desorption via the Redhead equation,[29] assuming first-order desorption and a coverage-independent desorption energy.

3. Data Analysis

To obtain information about the sticking coefficient, the adsorption and desorption rates, and the energetics of interaction of hydrocarbon molecules with the Au(111) surface using helium atom reflectivity, it is necessary to relate the measured specular reflectivity to the actual coverage of adsorbates. Depending on the spatial distribution of molecules on the surface, the relationship between measured specular signal (I) and actual coverage (θ) may be exponential, polynomial, or linear.[30] These coverage functions (see Figure 6) arise from changes in the effective cross-section of the adsorbates as the coverage increases. To determine the appropriate coverage function, ideally the sticking coefficient and monolayer density should be measured by Auger, LEED, or other techniques.[31]

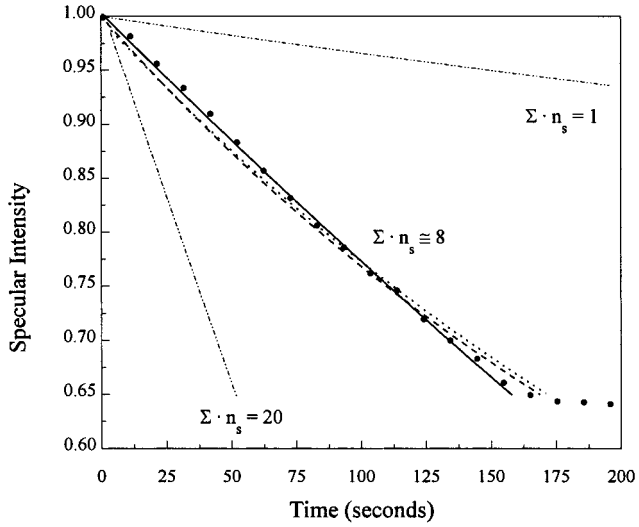

Figure 6. Simulation of specular intensity based on deposition conditions for a variety of growth models with the value of Σn_s optimized. Observed specular intensity (●), fully random adsorption (− −) $I = I_o\exp(-\theta\Sigma n_s)$, random on lattice sites (•••) $I = I_o(1-\theta)^{\Sigma n_s}$, islanding or repulsion (—) $I = I_o(1-(\theta\Sigma n_s))$. The outlying lines (—• •—) correspond to islanding adsorption but with Σn_s set equal to 1 and 20.

However, for alkane physisorption on transition metals, literature reported sticking coefficients are limited to studies of methane,[18] ethane,[11] and propane[10] on Pt(111). Thus, an alternate analysis technique was required to relate adsorbate populations to observed helium atom reflectivity.

At low coverages, the adsorption can be modeled by simple Langmuir adsorption. In this model, the number of blocked sites is directly proportional to the number of molecules adsorbed. As the coverage increases, fewer sites are available for adsorption and the overall adsorption rate will be reduced. At constant flux, this will be seen as a decrease in the rate of decay of specular intensity as a function of exposure. If the flux is known, the observed rate decrease can then be related to the surface coverage. When estimated coverages generated by this model are compared to specular intensities, the appropriate ordering model and a value for the product of scattering cross-section (Σ) and saturation coverage (n_s) can be identified. The absolute values of Σ, n_s, or the initial sticking coefficient (s_o) cannot be separately determined without performing several experiments at different fluxes and surface temperatures. Although the ordering model can be identified and a relative sticking coefficient and the product Σn_s can be found, individual parameter values cannot be assigned without additional information or assumptions.

With a rough estimate of the monolayer density, fluxes can be stated in terms of monolayers per unit time. For the systems examined in this paper, no measurements of the saturation coverage for physisorbed molecules were available for Au(111). However, densities for propane through octane on Pt(111) as determined by LEED[32] served as rough estimates. A linear extrapolation provided estimates of n_s for the longer chain hydrocarbons. The reciprocals of these densities were also used as an estimate for the hard-sphere cross-sections, which were in close agreement with cross-sectional areas reported for hydrocarbons adsorbed on graphite.[33]

3.1. Steady-State Coverage. Two approaches were used to relate the measured specular helium intensity to the hydrocarbon coverage on the Au(111) surface. The first approach relied on the generation of small steady-state coverages under particular dosing conditions. Adsorbate flux and surface temperature were selected so that the specular signal loss was typically 10−50%. With knowledge of an adsorption rate constant (k_a) and a desorption rate constant (k_d), the steady-state coverage (θ) can be calculated based on the assumption of Langmuir adsorption:

$$\frac{d\theta}{dt} = k_a(1-\theta) - k_d\theta \tag{1}$$

At steady-state, $d\theta/dt = 0$, and

$$k_a = \frac{k_d\theta}{(1-\theta)} \tag{2}$$

The rate of adsorption, which is equal to the product of the hydrocarbon impingement rate and the sticking coefficient (s), will be proportional to the partial pressure of the hydrocarbon vapor in the scattering chamber. To remove the need to know either the sticking coefficient or the ion gauge sensitivity, a second experiment with the same hydrocarbon can be performed at a higher flux than the first. If the surface temperature is unchanged (to maintain k_d across both experiments) and the coverage is not greatly increased (to approximately maintain s), a ratio is generated which is dependent only on the measured partial pressures.

$$\frac{p_1}{p_2} = \frac{\theta_1(1-\theta_2)}{\theta_2(1-\theta_1)} \tag{3}$$

To use eq 3 with experimental data, the measured partial pressures of the hydrocarbon vapor in the scattering chamber were substituted for p_1 and p_2. In the place of θ, one of the three surface ordering relations is expressed as a function of the observed intensity and the unknown quantity, Σn_s. Proper calibration is achieved when a coverage functional form and a value for Σn_s are found that consistently predict the specular intensity for a series of impingement rates at the same temperature.

3.2. Time-Dependent Coverage. The second approach for relating specular intensity to coverage was useful at low surface temperatures or high adsorbate fluxes, where the steady-state coverage was high. In this case, the time-dependent change in reflectivity must be monitored and related to the changing adsorbate coverage. Evaluation of the Langmuir differential equation (eq 1) with a clean crystal boundary condition that assumes that $\theta = 0$ at $t = 0$, generates the following time-dependent expression:

$$\theta = \frac{k_a}{k_a + k_d}(1 - \exp(-(k_a + k_d)t)) \tag{4}$$

This expression may be used to compute the coverage expected at any time during an experiment where the adsorption and desorption rate constants are known or can be estimated.

The desorption rate constant was determined using the Arrhenius equation and a desorption energy determined by TPD. Alternatively, at higher surface temperatures where desorption is significant, the desorption rate constant could be obtained from the half-life of the specular intensity recovery when adsorbate dosing was stopped. To obtain k_a, the Langmuir differential equation (eq 1) was evaluated at the limit of zero coverage where the rate of change of coverage is independent of the rate of desorption. Using these values for k_a and k_d, an expression for the time-dependent coverage in terms of the

measured specular intensity can be derived. This expression can then be fit to the specular intensity data with the appropriate ordering model, cross-section (Σ), and saturation coverage (n_s) extracted from the fit.

In Figure 6, a sample data set has been compared to this expression for three possible ordering models and selected values of Σn_s. For this particular experiment, the range of interest is from 30 to 150 s, where the pressure and consequently the adsorption rate was held constant. The rate of desorption was estimated from measurements of the desorption half-life performed after the initial dose. If we approximate the hard-sphere cross-section of the molecule as the reciprocal of the packing density, then Σn_s will be equal to one if the effective and hard-sphere cross-sections are equal. In the experiment shown in Figure 6, all ordering models with a cross-section approximately 8 times larger than the hard-sphere estimate provide reasonable fits to the data. However, both the exponential and polynomial curves first underestimate and then overestimate the observed specular intensity. The linear model fits the data better across a broader region of time. On the basis of analysis of many data sets of this type, the specular to coverage relationship used for adsorption at low coverage favors the linear, or islanding, model of monolayer growth with an adsorbate scattering cross-section approximately eight times larger than the hard-sphere estimate. For comparison, the effective scattering cross-section of CO on Pt(111) is at least 6 times the hard-sphere cross-section.[34]

3.3. Sticking Coefficients. Once the expression connecting the specular intensity to coverage has been determined, sticking coefficients can be derived. Since the initial sticking coefficient is defined as the rate of adsorption observed at the onset of dosing on a clean crystal divided by the impingement rate, sticking coefficients can be calculated entirely from observable quantities.

The impingement rate used in all calculations was estimated from an ion gauge measurement of the partial pressure of dose gas in the scattering chamber. To determine the actual partial pressure, a correction factor (S/S_{N2}) was applied to the ion gauge reading to compensate for the molecule-specific ease of ionization as well as degree of fragmentation. For the shorter chain hydrocarbons ($n \leq 7$) and some cyclic molecules, these factors were available in the literature.[35] However, for the longer chain hydrocarbons, the sensitivity factors had to be extrapolated from available data. Linear relationships of ion gauge sensitivity (S/S_{N2}) as a function of the number of carbon atoms in the chain, n, were determined by a least-squares fit to available data for the long-chain alkanes and alkenes.

$$S/S_{N_2} = 1.1n + 0.4 \qquad \text{(alkane)} \tag{5}$$

$$S/S_{N_2} = 1.1n \qquad \text{(alkene)} \tag{6}$$

For measured hydrocarbon partial pressures of $10^{-9}-10^{-7}$ Torr, the typical fluxes are estimated to range from 10^{11} to 10^{13} molecule·cm^{-2}·s^{-1}.

To determine the initial rate of adsorption, the initial slope of the curve of coverage versus time is used. This often provides a satisfactory estimate; however, the initial slope may also partially reflect the contribution of processes other than the basic molecule-ideal surface interaction. Preferential adsorption at steps or the influence of very small populations of contaminants may alter the observed coverage increase upon dosing. Also, the dosing flux must equilibrate rapidly before the slope is altered by the presence of molecules adsorbed on the surface.

TABLE 1: Activation Energies for Desorption of *n*-Alkanes and 1-Alkenes from Au(111)

chain length	*n*-alkanes (kJ/mol)	1-alkenes (kJ/mol)
1	14.5 ± 0.2	
2	24.1 ± 0.2	
4	40.5 ± 0.2	
6	55.9 ± 0.6	56.6 ± 0.9
7	62.7 ± 0.7	
8	69.7 ± 0.3	70.1 ± 0.3
9	75.2 ± 0.7	76.2 ± 0.7
10	80.1 ± 0.7	81.1 ± 0.7
11		87.8 ± 1.3
12	93.6 ± 0.5	

Since helium atom reflectivity is sensitive to extremely small populations of molecules, the initial adsorption slope arising from slow, low-flux dosing can be determined before significant site-blocking occurs. Only large molecules which stick to chamber walls and do not reach an equilibrium pressure within seconds, e.g., ($C_{16}H_{33}SH$) have been difficult to evaluate.

Although suitable for analysis at low surface temperatures, this simple approach begins to fail at surface temperatures close to the peak desorption temperature. This failure arises from the rapid decrease of the slope of the coverage versus time curve as the coverage approaches the steady-state population. As the surface temperature and the rate of desorption are increased, the steady-state population is reduced. As a result, the decay of the slope may begin within the region used to determine the initial slope. If a relatively large time interval is used to determine the slope, the resulting initial rate of adsorption will be an average of the true initial rate and subsequent, lower rates.

To compensate for both desorption and site-exclusion factors which can reduce the apparent rate of adsorption, the time-dependent Langmuir adsorption expression discussed previously was used. Since coverage (θ) is known from specular data, and the desorption rate constant (k_d) can be estimated based on surface temperature measurements, k_a can now be obtained by least-squares fit. As before, the experimental data from the first few seconds of dosing is preferably used to generate a rate of adsorption. However, using the time-dependent expression, the initial rate of adsorption can also be obtained from data outside the first few seconds of the experiment. Although other cooperative effects such as adsorbate-assisted adsorption may cause deviations from the true initial value, the flexibility provided by this technique is useful to analyze experiments that may have pressure spikes or other flaws at the onset of dosing.

4. Results and Discussion

4.1. Energies of Adsorption. The measured activation energies for desorption from Au(111) for the linear hydrocarbons studied are summarized in Table 1. For the long-chain members ($n \geq 6$) of both series, there is a linear increase of 6.2 ± 0.2 kJ/mol additional adsorption energy per methylene unit. For the *n*-alkanes, there is a 19.0 ± 1.1 kJ/mol zero offset arising in part from differences between the methyl and methylene subunits. For the 1-alkenes, the zero offset is slightly greater, 20.0 ± 1.3 kJ/mol. When compared to bulk properties such as the heat of vaporization or the average polarizability, the measured energies scale proportionally, pointing to the physical nature of the molecular interaction with the surface.

Although direct comparison between the short-chain and long-chain alkanes are complicated by the absence of methylene groups in methane and ethane, the smaller alkanes are, in proportion, more strongly bound to the surface than their longer chain counterparts. The incremental adsorption energy per

additional carbon decreases from 9.6 kJ/mol for ethane to 8.2 kJ/mol for butane to 7.7 kJ/mol for hexane before reaching the asymptotic value of 6.2 kJ/mol.

For the alkane series, the measured activation energies for desorption are similar to adsorption energies reported in the literature for alkanes deposited on metals other than gold (Figure 1). A linear increase of adsorption energy with chain length is indicative that the adsorbate is oriented with the molecular plane (as defined by the backbone of carbon atoms) aligned parallel to the surface. If this alignment was rotated by 90° about the long molecular axis, the methylene groups would be alternatively arranged in high and low positions above the surface. Extending the chain with additional methylenes would give rise to an odd−even chain length effect which would be observed as an alternating series of small and large increases of adsorption energy. Alternatively, placement of the molecule with the long molecular axis normal to the surface would show only a minimal increase of adsorption energy since additional methylene units would be located too far from the surface to contribute to the measured activation energy for desorption.

Desorption experiments with a series of unsaturated hydrocarbons were performed to explore the dependence of the adsorption energy on the degree of unsaturation of the molecule as well as the location of the double bond (Table 2). In particular, the activation energies for desorption of a series of butenes (*trans*-2-butene, *cis*-2-butene, and 2-methylpropene) demonstrated (in agreement with ref 15) that the location of the double bond within the molecule does affect the adsorption energy by a few kJ/mol.

For physisorption, the attractive interaction between the adsorbate and the substrate is due to van der Waals forces. As the molecule approaches the surface, a correlation arises between the instantaneous dipole fluctuations present in the metal and those present in the molecule. As a result, the magnitude of this attraction can be related to the polarizability of the molecule. Since polarizability is known to be an additive property,[36] an empirical energy model was developed to rationalize the data and to provide predictions of the activation energies for desorption based on molecular composition.

4.2. Bond Additive Model. 4.2.1. Choice of Parameters. Since the total polarizability of hydrocarbons can be predicted (to within ~1% accuracy) by associating a certain amount of polarizability to each carbon−hydrogen and carbon−carbon bond, a model was constructed to determine the contribution of each bond to the activation energy for desorption observed for the molecules examined here. To account for the measured values for the first few members of the alkane and alkene series, it was necessary to base the contribution of each bond to the adsorption energy on its location within the molecule (see Figure 7 where heptane, the first hydrocarbon containing an "asymptotic" methylene group, is shown). Since the incremental methylene contribution does not reach its asymptotic value before heptane, four carbon species are required for the model, resulting in four types of carbon−hydrogen bonds and three types of carbon−carbon bonds (Table 3).

Methane, consisting of four carbon−hydrogen bonds, can be used to calculate the adsorption energy contribution of a carbon−hydrogen bond located at the end of the molecule ($E_{\mathrm{Type1C-H}} = 3.6$ kJ/mol). With this value and the activation energy for desorption of ethane, the contribution of a carbon−carbon bond originating from an end carbon atom can also be calculated ($E_{\mathrm{Type1-2C-C}} = 24.1 - 6 \times 3.6 = 2.5$ kJ/mol). For all locations within the molecule, the ratio of the two contributions ($E_{\mathrm{C-C}}/E_{\mathrm{C-H}} = 1.44$) will be assumed to be constant.

TABLE 2: Activation Energies for Desorption of Double Bonded Species from Au(111)

molecule	observed energy (kJ/mol)
ethylene	27.0 ± 0.2
benzene	57.9 ± 0.2
trans-2-butene	41.7 ± 0.2
cis-2-butene	44.5 ± 0.2
2-methylpropene	45.4 ± 0.2

Figure 7. Schematic of a heptane molecule showing atom and bond numbering for the additive model. Carbon atoms are numbered toward the core of the molecule. The contribution of all carbons numbered greater than three are considered to be "asymptotic".

TABLE 3: Additive Model Components (see Figure 7 for Legend)

species	energy contribution (kJ/mol)
type 1 C−H Bond	3.6
type 2 C−H Bond	3.2
type 3 C−H Bond	2.8
asymptotic C−H Bond	2.3
type 1−2 C−C Bond	2.5
type 2−3 C−C Bond	2.0
asymptotic C−C Bond	1.6
double bond	10.5
sulfur atom	24.1
S−H bond	8.1

Using this ratio, the asymptotic methylene contribution of 6.2 kJ/mol can be partitioned between two carbon−hydrogen bonds (2.3 kJ/mol each) and one carbon−carbon bond (1.6 kJ/mol). For simplicity, the contributions of the intermediate carbon−hydrogen and carbon−carbon bonds have been linearly interpolated from the methyl and methylene extreme values (Figure 7). To reflect the intermediate nature of bonds located in cyclic molecules, the activation energy for desorption can be calculated as the sum of the contributions of intermediate bonds (Type 2 C−H bonds and Type 2−3 C−C bonds).

Using these additive bond contributions and the experimental activation energy for the desorption of 1-octene, the double bond contribution can be derived to be 10.5 kJ/mol. Although this model will not distinguish between double bonds with differing positions within the molecule, its performance for both saturated and unsaturated hydrocarbons is quite satisfactory and will be discussed in the following section.

4.2.2. Model Performance. The comparison between the observed and calculated activation energies for desorption is presented in Table 4. Since the energy of physisorption depends on an additive property, i.e., the polarizability, it is not surprising that this additive model predicts the observed activation energy for desorption relatively well. The model, which contains four free parameters,[37] accounts for the experimental energies of 25 saturated and unsaturated hydrocarbons with an average error of 1.9%. Of these 25 molecules, 84% of the measured adsorption energies differ from the calculated values by less than twice the average error. It is the deviation of the model predictions from experimental values that is likely to provide the most useful information. The greatest error occurs for ethylene and 1,3-butadiene, with underestimation of the activation energy for desorption by 5−8%. The origin of this error appears to be analogous to the end effect in the saturated chains. Having determined the contribution of the double bond from a

TABLE 4: Additivity Model Comparison to Data

molecule	observed energy (kJ/mol)	calculated energy (kJ/mol)	deviation (% error)
methane	14.5	14.4	fitted
ethane	24.1	24.1	fitted
butane	40.5	41.4	2.2
hexane	55.9	56.2	0.5
heptane	62.7	62.4	−0.5
octane	69.7	68.6	−1.6
nonane	75.2	74.8	−0.5
decane	80.1	81.0	1.1
dodecane	93.6	93.4	−0.2
ethylene	27.0	24.9	−7.8
trans-2-butene	41.7	43.5	4.3
cis-2-butene	44.5	43.5	−2.2
2-methylpropene	45.4	44.3	−2.4
1-hexene	56.6	57.4	1.4
1-octene	70.1	69.8	−0.4
1-nonene	76.2	76.0	−0.3
1-decene	81.1	82.2	1.4
1-undecene	87.8	88.4	0.7
cyclohexane	50.6	50.4	−0.4
cyclooctane	63.1	67.2	6.5
benzene	57.9	56.7	−2.1
toluene	66.1	66.3	0.3
propylene	35.0	34.2	−2.2
allene	34.2	35.4	3.5
1,3-butadiene	46.2	43.8	−5.2
thiophene	60	59.9	−0.2
ethanethiol	57	52.1	−8.6
butanethiol	68	68.1	0.1
hexanethiol	79	81.5	3.1
octanethiol	87	93.9	7.9
nonanethiol	103	100.1	−2.8
tetradecanethiol	150	131.1	−13[a]
octadecanethiol	158	155.9	−1.3
docosanethiol	169	180.7	6.9
diethyl sulfide	68	63.5	−6.6
dibutyl sulfide	86	91.1	5.9

[a] This molecule has been omitted from the calculation of the average error (see text).

long-chain 1-alkene (a molecule with both an unsaturated region and a large saturated region) some deviation may be expected for the smaller alkenes. It is possible that this end effect deviation may result from the deformation of the charge density of the metal surface around the adsorbed molecule which would have a larger effect on the ends of the molecule than on the center.[38] This view is confirmed by the fact that good agreement between experiment and model is achieved for cyclohexane and benzene but not for cyclooctane. To obtain better agreement for this molecule, the contribution of the carbon−hydrogen and carbon−carbon bonds should be smaller, i.e., closer to the asymptotic value. The trend is, therefore, explainable since the increased size of the ring in the limit of a very large cycloalkane would create an environment similar to that of a long linear alkane.

4.2.3. Extension to Sulfur-Containing Molecules. To test the model on a wider range of molecules, the data on the activation energy for desorption of alkanethiols and other sulfur-containing molecules which were collected on this apparatus and reported in an earlier paper[17] were reexamined. The value for the sulfur atom contribution was determined from the difference in the *y*-offsets of the alkane and alkanethiol series as 24.1 kJ/mol. For simplicity, this value was also assumed to be constant for all molecules. The contribution of the sulfur−hydrogen bond was determined to be 8.1 kJ/mol from the alkanethiol data as the average difference between each observed activation energy for desorption and the sum of the contribution of the known components (carbon−carbon bonds, carbon−hydrogen bonds, and sulfur atoms of that particular molecule). For the present purpose, the carbon atoms have been numbered as if the sulfur was a carbon atom.

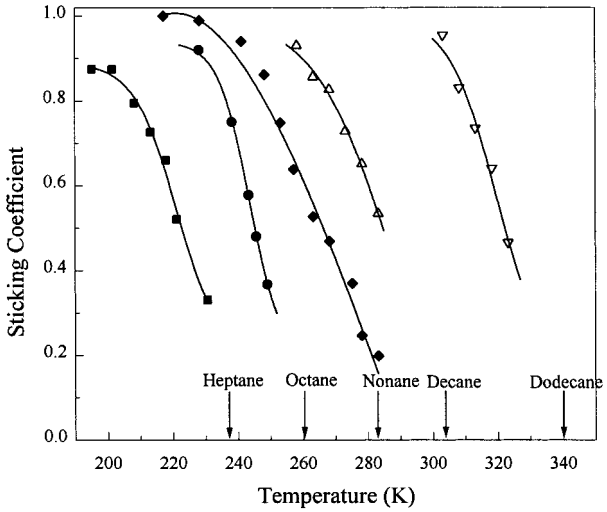

Figure 8. The sticking coefficients as a function of absolute temperature are shown for the *n*-alkanes: heptane (◆), octane (●), nonane (◆), decane (△), dodecane (▽). Arrows correspond to the peak desorption temperature determined during reflectivity detected TPD measurements for each molecule.

The agreement between the experimental and calculated adsorption energies for the sulfur-containing molecules is somewhat worse than that for the hydrocarbons. While this could be expected because of the simplicity of the model, the calculated adsorption energies of both ethanethiol and tetradecanethiol deviate sufficiently from the experimental data to warrant a closer look.

For ethanethiol, the model severely underpredicts the activation energy for desorption (8.6%). As ethanethiol is the shortest alkanethiol studied, potentially this deviation is due to the same "end effect" as observed with the alkanes and alkenes. However, the even larger underprediction of tetradecanethiol (13%) is likely to be due to an entirely different cause, i.e., experimental error). For long chain-lengths the incremental energy per additional methylene group (as found in the hydrocarbon series) is asymptotically constant. As a result, the experimental activation energy for desorption of tetradecanethiol, which lies well above the linear best-fit that represents most of the other alkanethiols, is very likely to be incorrect, (i.e., too high).

4.3. Sticking Coefficients. At low temperatures, the initial sticking coefficient (s_o) is near unity for all the hydrocarbons tested. However, a decrease in sticking coefficient is observed as the surface temperature is increased. This effect does not become pronounced until the surface temperature is approximately 50 K below the temperature corresponding to the observed TPD desorption peak of each species. At surface temperatures above the characteristic TPD temperature, the sticking coefficient approaches zero (Figure 8).

To compare the sticking behavior of different molecules, the actual surface temperatures were converted to a reduced temperature, T^*. This reduced temperature is calculated as the ratio of the actual surface temperature to the peak desorption temperature as observed by TPD for each species. When the sticking coefficients are replotted as a function of the reduced temperature, the sticking coefficient curves overlap for all the *n*-alkanes and 1-alkenes (Figure 9) indicating that the mechanism of adsorption is independent of the identity of the adsorbate.

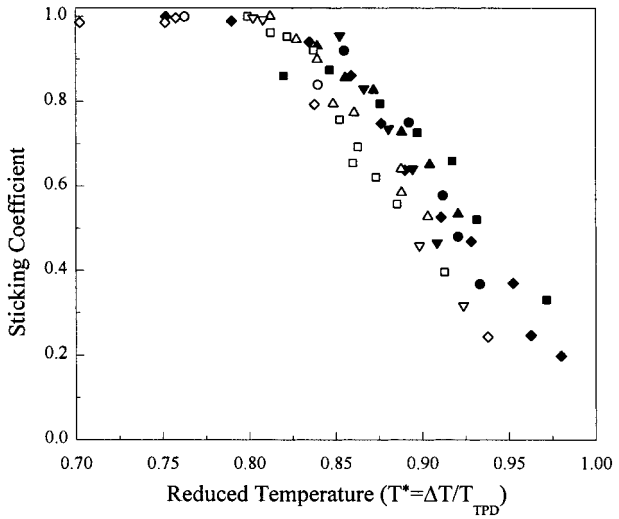

Figure 9. The sticking coefficient of *n*-alkanes (filled) and 1-alkenes (open) as a function of reduced temperature relative to the TPD peak for each molecule.

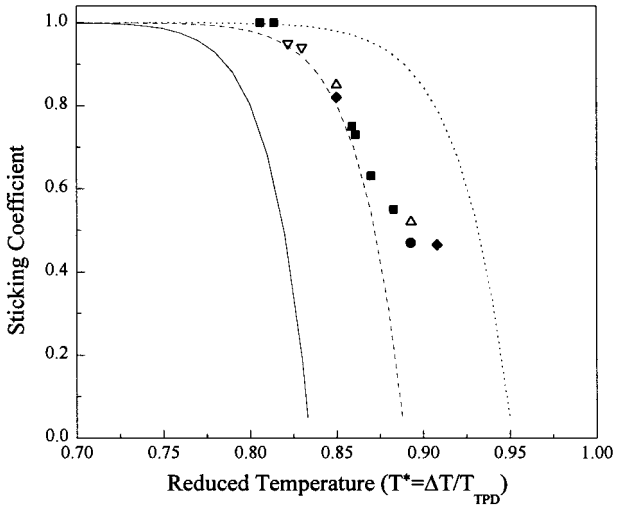

Figure 10. The sticking coefficient of 1-hexene as a function of reduced temperature for a series of approximate dosing rates: 5×10^{-4} ML/s (▽), 2×10^{-3} ML/s (◆), 5×10^{-3} ML/s (◆), 8×10^{-3} ML/s (●), 5×10^{-2} ML/s (△). Condensation coefficients were also calculated using the model of Brown et al.[20] modified for first-order desorption and a temperature-independent sticking coefficient equal to one: 5×10^{-4} ML/s (—), 5×10^{-3} ML/s (− −), 5×10^{-2} ML/s (···).

Similar results have also been observed using the same apparatus for the physisorption of 1-alkanethiols comprised of two to 10 carbons.

A similar sticking coefficient dependence on surface temperature was observed by Arumainayagam et al.[11] in their studies of the adsorption of ethane on Pt(111). At surface temperatures close to the desorption temperature, trapping probabilities as measured by the technique of King and Wells were observed to decrease significantly. According to hard-cube models, trapping probability should have had little dependence on surface temperature so the differences were attributed to desorption within the experimental time resolution of one second. To quantify the desorption effects, a model was generated to predict the apparent trapping coefficient for a system where the true sticking coefficient was unity, independent of temperature. Although the model successfully accounted for the general shape of the trapping coefficient curve as a function of surface temperature (shown in Figure 9 of ref 11), a deviation from observed data still remained which was significant only at surface temperatures close to the desorption temperature (across the range $T^* = 0.75-1.0$).

An estimate of the sticking coefficient as a function of surface temperature can be generated from the data and model of Arumainayagam et al.[11] by calculating the ratio of the observed trapping probabilities divided by the predicted trapping probabilities. Since the model accounts for the reduction in the apparent trapping probability due to desorption, any deviation from the predicted values will be real. For low surface temperatures, there is no deviation between the observed data and the model, and a sticking coefficient of one can be calculated. However, at surface temperatures closer to the peak desorption temperature (160 K), the observed and predicted trapping probabilities diverge. When the estimated sticking coefficients generated in this way are plotted as a function of reduced temperature, the resulting plot appears similar to the long chain alkane sticking coefficient data determined in this study.

Due to the qualitatively similar appearance of the effects of desorption and the observed dependence of the sticking coefficient on surface temperature, it was necessary to determine whether sticking coefficients or condensation coefficients were being measured using the techniques outlined in section 3.2. Whereas the condensation coefficient is dependent on the process of desorption (because it measures the net change in adsorbate population per unit flux), the sticking coefficient measures only the probability of adsorption independently from the flux. As a result, the sticking coefficient will be independent of both the impingement rate and the rate of desorption.

In an extensive study of the adsorption of water on ice multilayers, Kay and collaborators[20] observed the dependence of the condensation coefficient on surface temperature and flux while the sticking coefficient remained unity. By increasing the surface temperature (and consequently, the rate of desorption), the condensation coefficient decreased from unity to zero. However, as flux was increased, the measured condensation coefficient also increased for a given surface temperature. By comparison, examination of sticking coefficient data collected for 1-hexene across approximately 2 decades of flux shows no sticking coefficient dependence on flux (Figure 10). This provides evidence that the true sticking coefficients are being reported here.

Using the data analysis procedure presented in this paper, no additional modeling is required to modify or normalize the observed sticking coefficients. With the technique of helium atom scattering, surface populations are measured directly during dosing so there is no dead-time before measurements when desorption may reduce the actual quantity of adsorbates. Any effects of desorption on coverage have already been fully accounted for by the Langmuir adsorption model used to derive the sticking coefficient values. If desorption rates were systematically estimated incorrectly (due to miscalibration of the surface temperature thermocouple for example), sticking coefficients measured at surface temperatures where desorption is significant would depend on the incoming flux. Similarly, if impingement rates are inaccurate, measurements of sticking at low surface temperatures would deviate from unity.

The origin of the decrease in sticking coefficient therefore appears to be due to incomplete accommodation of the molecule by the Au(111) surface at higher temperatures. Even though the adsorbate molecules are only arriving with an average of 3.6 kJ/mol of translational energy (from $E = {}^3/_2kT$ at 300 K), this quantity is sufficient to allow the molecule to avoid physisorption at surface temperatures near the peak desorption

temperature. At low temperature, both phonon creation and intramolecular energy transfer from translational to rotational (and less likely, vibrational modes) can allow the molecule to become trapped in the physisorption well of the surface. However, at higher surface temperatures, the surface is unable to readily accept energy from the molecule resulting in incomplete accommodation.

From this set of results, it is unclear whether the procedure of dosing from ambient background gas instead of from a monoenergetic molecular beam has affected the values of the reported sticking coefficients. For ethane, the sticking coefficients derived from the results of Arumainayagam et al.[11] show no dependence on translational energy between 10 and 24 kJ/mol. Therefore, it is unlikely that the observed decrease in sticking coefficient at higher surface temperatures is a result of increasingly selective physisorption of less translationally energetic molecules.

5. Summary

The kinetics and energetics of the physisorption of thermal energy *n*-alkanes and 1-alkenes on Au(111) has been determined. For both systems, adsorption on the surface proceeds through a physisorbed state and can be modeled using Langmuir first-order adsorption kinetics. At higher surface temperatures, the physisorption sticking probability is decreased due to incomplete accommodation by the surface for both hydrocarbon series.

For the long chain-hydrocarbons, the contribution of each additional methylene group to the activation energy for desorption from a physisorbed state is 6.2 ± 0.2 kJ/mol. All molecules studied, both linear and cyclic bind with the molecular plane oriented parallel to the surface. A bond-additive empirical model has been presented which is able to predict the observed physisorption energies for 25 hydrocarbons with an average error of less than 2.0%. If sulfur-substituted hydrocarbons are also considered, the average error increases to 2.6% (for 35 molecules).

The physisorption sticking coefficient has been established for straight chain alkanes and alkenes across a range of temperatures. For molecules incident with thermal kinetic energy (as generated by dosing through a leak valve), the initial sticking coefficient is near unity at low temperatures. This value decreases as the surface temperature is raised closer to the temperature corresponding to the observed TPD desorption peak. Even after a higher rate of desorption is accounted for, a decrease in sticking can be seen. This temperature-dependent behavior is similar for all linear molecules studied.

To generate the sticking coefficients from the measured specular helium reflectivity data, a series of equations for the calibration of specular intensity to coverage have been presented. These equations can determine the conversion relationship for experiments where dosing partial pressure and specular signal are recorded as a function of time. Without prior knowledge of the sticking coefficient, the mathematical form of the ordering relationship as well as relative values of the parameters can be determined by best-fit of recorded data. Several experiments performed at different temperatures and dose fluxes provide enough information to calculate scattering cross-section and to determine the ordering mode. Once the specular signal intensity is converted to coverage, sticking coefficients can be calculated by modeling the rate of adsorbate population change.

Acknowledgment. The partial support of the National Science Foundation (Grants CHE-9619190 and DMR-9400362) and the Department of Energy (DE-FG02-93ER45503) for this research is gratefully acknowledged. It is a pleasure to thank A. Levi and I. Siepmann for useful discussions. The assistance of P. Schwartz in the operation of the low temperature helium beam scattering apparatus is gratefully acknowledged.

References and Notes

(1) See references in Somorjai, G. A. *Chemistry in Two Dimensions: Surfaces*; Cornell University Press: Ithaca, NY, 1981, and Somorjai, G. A. *Introduction to Surface Chemistry and Catalysis;* John Wiley and Sons: New York, 1994.

(2) Chesters, M. A.; Somorjai, G. A. *Surf. Sci.* **1975**, *52*, 21.

(3) Hamza, A. V.; Steinruck, H. P.; Madix, R. J. *J. Chem. Phys.* **1987**, *86*, 6506.

(4) Schoofs, G. R.; Arumainayagam, C. R.; McMaster, M. C.; Madix, R. *Surf. Sci.* **1989**, *215*, 1.

(5) Ceyer, S. T. *Annu. Rev. Phys. Chem.* **1988**, *39*, 479 and references therein.

(6) Balasubramanian, S.; Klein, M. L.; Siepmann, J. I. *J. Phys. Chem.* **1996**, *100*, 11960.

(7) Gupta, S.; Koopman, D. C.; Westermann-Clark, G. B.; Bitsanis, I. A. *J. Chem. Phys.* **1994**, *100*, 8444.

(8) Sullivan, D. J. D.; Flaum, H. C.; Kummel, A. C. *J. Phys. Chem.* **1993**, *97*, 12051.

(9) Sexton, B. A.; Hughes, A. E. *Surf. Sci.* **1984**, *140*, 227.

(10) McMaster, M. C.; Arumainayagam, C. R.; Madix, R. J. *Chem. Phys.* **1993**, *177*, 461.

(11) Arumainayagam, C. R.; Schoofs, G. R.; McMaster, M. C.; Madix, R. J. *J. Phys. Chem.* **1991**, *95*, 1041.

(12) McMaster, M. C.; Schroeder, S. L. M.; Madix, R. J. *Surf. Sci.* **1993**, *297*, 253.

(13) Kang, H. C.; Mullins, C. B.; Weinberg, W. H. *J. Chem Phys.* **1990**, *92*, 1397.

(14) Brand, J. L.; Arena, M. V.; Deckert, A. A.; George, S. M. *J. Chem. Phys.* **1990**, *92*, 5136.

(15) Teplyakov, A. V.; Gurevich, A. B.; Yang, M. X.; Bent, B. E.; Chen, J. G. *Surf. Sci.* **1998**, *396*, 340.

(16) Dubois, L. H.; Zegarski, B. R.; Nuzzo, R. G. *J. Am. Chem. Soc.* **1990**, *112*, 570.

(17) Lavrich, D. J.; Wetterer, S. M.; Bernasek, S. L.; Scoles, G. *J. Phys. Chem. B* **1998**, *112*, 3456.

(18) Arumainayagam, C. R.; McMaster, M. C.; Schoofs, G. R. *Surf. Sci.* **1989**, *222*, 213.

(19) Stinnett, J. A.; Madix, R. J. *J. Chem. Phys.* **1996**, *105*, 1609.

(20) Brown, D. E.; George, S. M.; Huang, C.; Wong, K. L.; Rider, K. B.; Smith, R. S.; Kay, B. D. *J. Phys. Chem.* **1996**, *100*, 4988.

(21) Poelsema, B.; de Zwart, S. T.; Comsa, G. *Phys. Rev. Lett.* **1982**, *49*, 578.

(22) Smith, D. L.; Merrill, R. P. *J. Chem. Phys.* **1970**, *52*, 5861.

(23) Ibáñez, J.; García, N. *Phys. Rev. B* **1983**, *28*, 3164.

(24) Poelsema, B.; Palmer, R. L.; Comsa, G. *Surf. Sci.* **1984**, *136*, 1.

(25) Schwartz, P.; Schrieber, F.; Eisenberger, P.; Scoles, G. *Surf. Sci.* **1998**. To be published.

(26) Schwartz, P. Ph.D. Thesis, Princeton University Press, Princeton, NJ, 1998.

(27) Glebov, A.; Toennies, J. P.; Weiss, H. *Surf. Sci.* **1996**, *351*, 200.

(28) Borolani, V.; Celli, V.; Franchini, A.; Idiodi, J.; Santoro, G.; Kern, K.; Poelsema, B.; Comsa, G. *Surf. Sci.* **1989**, *208*, 1.

(29) Redhead, P. *Vacuum* **1965**, *12*, 203.

(30) Poelsema, B.; Comsa, G. *Faraday. Discuss. Chem. Soc.* **1985**, *80*, 247.

(31) Poelsema, B.; Comsa, G. *Scattering of Thermal Energy Atoms from Disordered Surfaces*; Springer-Verlag: New York, 1989.

(32) Firment, L. E.; Somorjai, G. A. *J. Chem. Phys.* **1977**, *68*, 2901.

(33) McClellan, A. L.; Harnsberger, H. F. *J. Colloid Interface Sci.* **1967**, *23*, 577.

(34) Poelsema, B.; Palmer, R. L.; De Zwart, S. T.; Comsa, G. *Surf. Sci.* **1983**, *126*, 641.

(35) Summers, R. *NASA Technical Note TN D-5285*, **1969**.

(36) Le Fèvre, C. G.; Le Fèvre, R. J. W.; Rao, B. P.; Smith, M. R. *J. Chem. Soc.* **1959**, 1188.

(37) We calculated the number of parameters chosen to optimize the fit (4) as follows: (1) the terminal C−H contribution from methane, (2) the terminal C−C contribution from ethane, (3) the asymptotic C−H and C−C contribution from the slope of best linear fit of the activation energy for desorption versus chain length, and (4) the C═C contribution from 1-octene. The other C−H and C−C bond contributions are interpolated and therefore are not considered as "free" parameters.

(38) Levi, A.; Scoles, G. **1998**. Unpublished work.

(39) Majer, V.; Svoboda, V. *Enthalpies of Vaporization of Organic Compounds*; Blackwell Scientific Publications: Boston, MA, 1985; pp 73−86.